## Electronic Supplementary Information (ESI)

# Local Structural Distortions and Reduced Thermal Conductivity in Ge-Substituted Chalcopyrite

Sahil Tippireddy[1], Feridoon Azough[2], Vikram[1], Animesh Bhui[3], Philip Chater[4], Demie Kepaptsoglou[5,6], Quentin Ramasse[5,7], Robert Freer[2], Ricardo Grau-Crespo[1], Kanishka Biswas[3], Paz Vaqueiro[1], and Anthony V. Powell[1*]

[1]*Department of Chemistry, University of Reading, Whiteknights, Reading, RG6 6DX, United Kingdom.*

[2]*Department of Materials, University of Manchester, Manchester, M13 9PL, United Kingdom.*

[3]*New Chemistry Unit, Jawaharlal Nehru Centre for Advanced Scientific Research, Jakkur, Bangalore-560064, India.*

[4]*Diamond Light Source, Harwell Science and Innovation Campus, Didcot OX11 0DE, United Kingdom.*

[5] *SuperSTEM Laboratory, SciTech Daresbury Campus, Daresbury WA4 4AD, United Kingdom*

[6] *Department of Physics, University of York, York YO10 5DD, United Kingdom*

[7] *School of Chemical and Process Engineering, University of Leeds, Leeds LS2 9JT, United Kingdom*

*Corresponding author: a.v.powell@reading.ac.uk

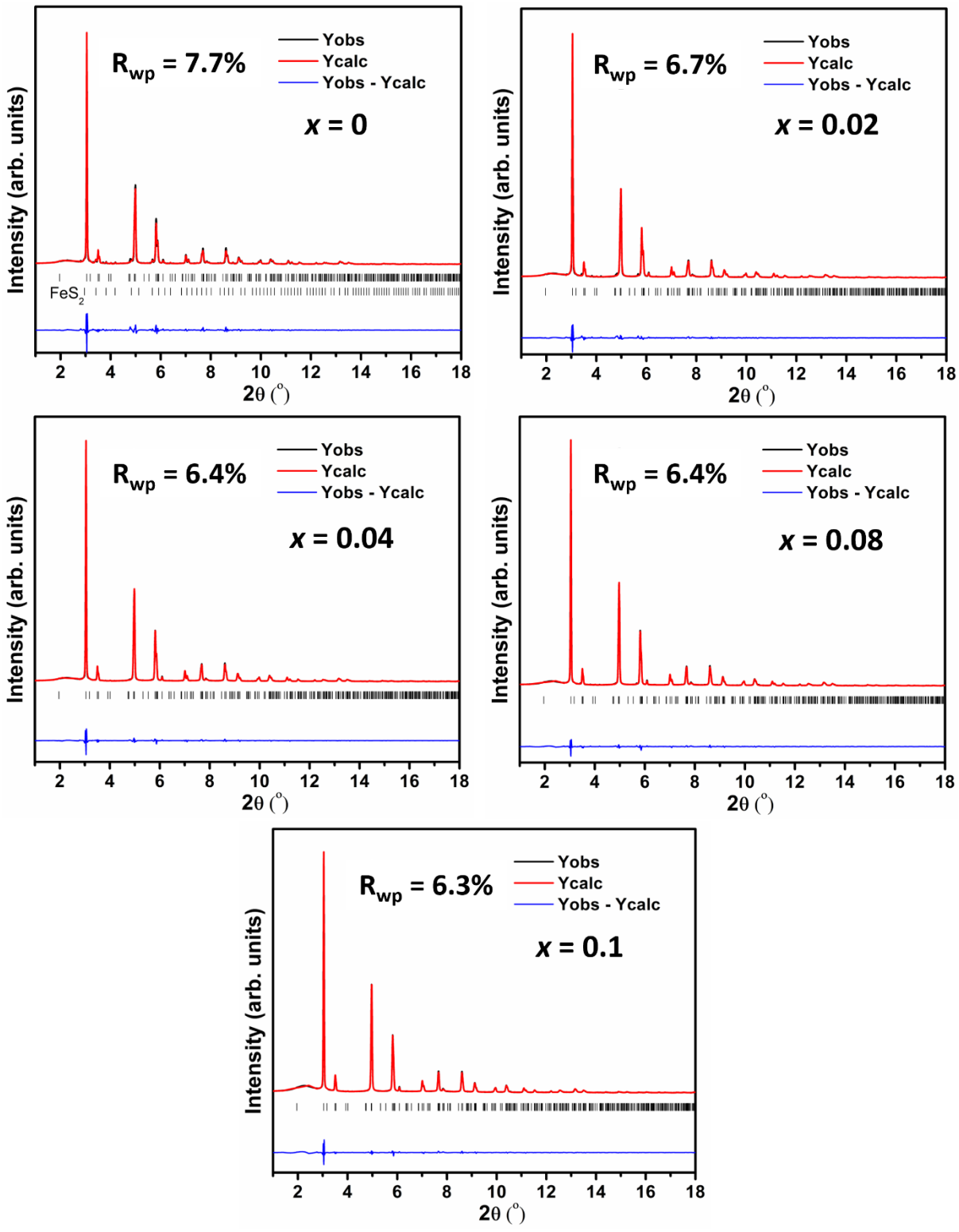


**Figure S1**. Rietveld refinement using synchrotron X-ray powder diffraction data (λ = 0.161669 Å) for $CuFe_{1-x}Ge_xS_2$ ($0 \leq x \leq 0.1$).

**Table S1**. Lattice parameters of $CuFe_{1-x}Ge_xS_2$ ($0 \leq x \leq 0.1$) described in the space group $I\bar{4}2d$.

| Sample | *a*/Å | *c*/Å |
|---|---|---|
| $CuFeS_2$ | 5.2909(3) | 10.4319(7) |
| $CuFe_{0.98}Ge_{0.02}S_2$ | 5.2912(2) | 10.4374(6) |
| $CuFe_{0.96}Ge_{0.04}S_2$ | 5.2913(2) | 10.4529(5) |
| $CuFe_{0.94}Ge_{0.06}S_2$ | 5.2918(2) | 10.4709(6) |
| $CuFe_{0.92}Ge_{0.08}S_2$ | 5.2913(2) | 10.4790(6) |
| $CuFe_{0.9}Ge_{0.1}S_2$ | 5.2903(3) | 10.4911(7) |

**Table S2**: Compositions[#] of the chalcopyrite-type phase determined by EDS.

| Sample (Ge concentration) | Nominal composition | EDS composition of the main phase* |
|---|---|---|
| $x = 0$ | $CuFeS_2$ | $Cu_{1.117(9)}\ Fe_{1.018(5)}S_2$ |
| $x = 0.02$ | $CuFe_{0.98}Ge_{0.02}S_2$ | $Cu_{1.146(5)}Fe_{0.984(5)}Ge_{0.024(3)}S_2$ |
| $x = 0.04$ | $CuFe_{0.96}Ge_{0.04}S_2$ | $Cu_{1.146(8)}Fe_{0.971(9)}Ge_{0.042(4)}S_2$ |
| $x = 0.06$ | $CuFe_{0.94}Ge_{0.06}S_2$ | $Cu_{1.118(4)}Fe_{0.957(5)}Ge_{0.062(3)}S_2$ |
| $x = 0.08$ | $CuFe_{0.92}Ge_{0.08}S_2$ | $Cu_{1.102(2)}Fe_{0.936(9)}Ge_{0.078(3)}S_2$ |
| $x = 0.1$ | $CuFe_{0.9}Ge_{0.1}S_2$ | $Cu_{1.098(3)}Fe_{0.912(2)}Ge_{0.094(2)}S_2$ |

*Normalized to 2 sulfur atoms per formula unit in $CuFeS_2$.

[#]Due to the overlap of the $K_\alpha$ and $L_\alpha$ characteristic lines of Cu and Fe, there may be uncertainties in the quantitative at.% determined by EDS.

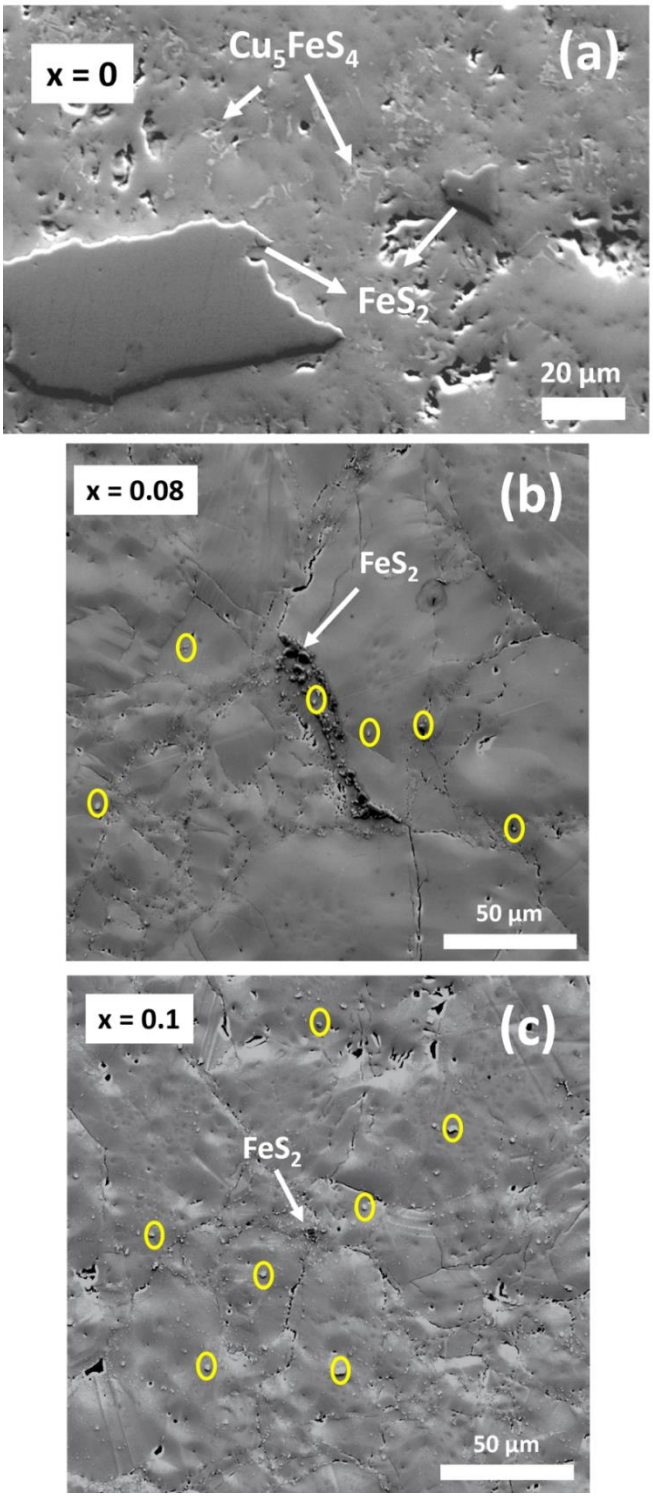


**Figure S2.** SEM images of $CuFe_{1-x}Ge_xS_2$ ($x$ = 0, 0.08 and 0.1) showing the presence of trace amounts of secondary phases. Substituted samples with higher Ge content ($x \geq 0.08$) contain another chalcopyrite-like phase (yellow circles) identified from EDS as $Cu_{21.69}Fe_{25.74}Ge_{0.94}S_{51.64}$ and $Cu_{21.91}Fe_{25.46}Ge_{1.83}S_{50.79}$ in materials with compositions $x$ = 0.08 and 0.1, respectively.

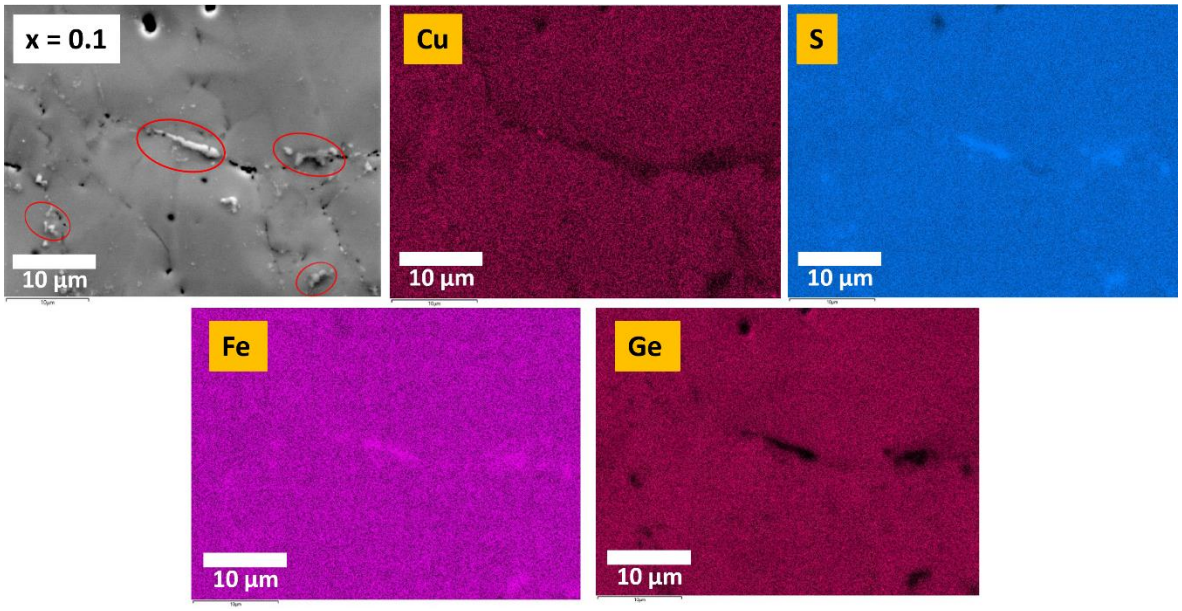


**Figure S3.** SEM-EDS elemental mapping of $CuFe_{0.9}Ge_{0.1}S_2$ showing the presence of copper-poor chalcopyrite-like secondary phase.

**Table S3**. XPS binding energies and corresponding oxidation states of individual elements in Ge-substituted $CuFe_{0.94}Ge_{0.06}S_2$.

| Element | Peak | B.E(eV)* | Oxidation state |
|---|---|---|---|
| **Cu** | $2p_{3/2}$ | 932.3 | +1 |
| | $2p_{1/2}$ | 952.1 | +1 |
| **Fe** | $2p_{3/2}$ | 710.2 | +3 |
| | $2p_{1/2}$ | 723.7 | +3 |
| | 2p | 707.9 | +2 |
| **S** | $2p_{3/2}$ | 161.4 | -2 |
| | $2p_{1/2}$ | 162.6 | -2 |
| **Ge** | $3d_{5/2}$ | 31.2 | +4 |
| | $3d_{3/2}$ | 31.8 | +4 |
| | $3d_{5/2}$ | 30.5 | +2 |
| | $3d_{3/2}$ | 31.1 | +2 |

*The binding energy of the XPS peaks is assigned on the basis of data in the literature[1-5] and in the NIST database.[6]

**Table S4**. Hall coefficient data for $CuFe_{1-x}Ge_xS_2$ ($0 \leq x \leq 0.1$) at room temperature.

| Sample | Charge carrier concentration ($\times 10^{19}$ cm$^{-3}$) | Charge carrier mobility (cm$^2$ V$^{-1}$ s$^{-1}$) |
|---|---|---|
| $CuFeS_2$ | 1.4(2) | 15(3) |
| $CuFe_{0.98}Ge_{0.02}S_2$ | 2.3(2) | 11(1) |
| $CuFe_{0.96}Ge_{0.04}S_2$ | 3.1(3) | 9(2) |
| $CuFe_{0.94}Ge_{0.06}S_2$ | 4.7(3) | 8(2) |
| $CuFe_{0.92}Ge_{0.08}S_2$ | 2.8(4) | 11(1) |
| $CuFe_{0.9}Ge_{0.1}S_2$ | 1.9(2) | 15(2) |

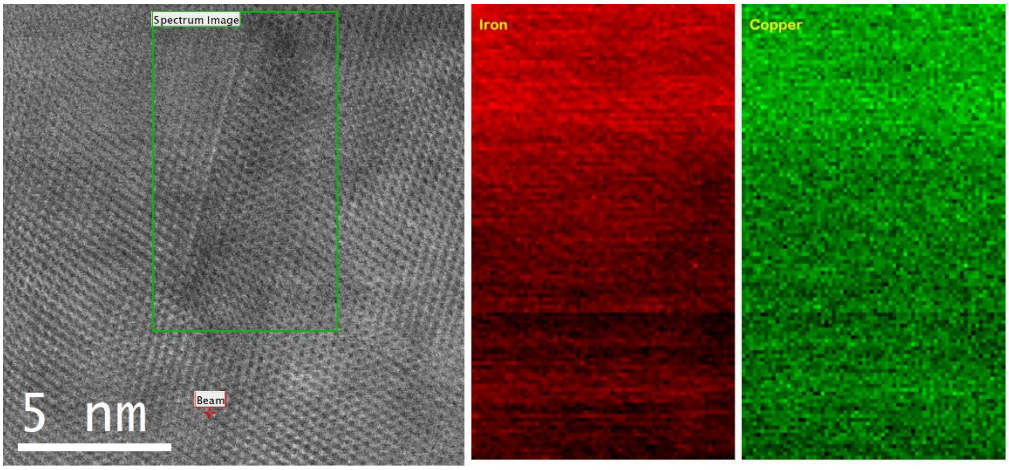


**Figure S4**. STEM image illustrating the chemical homogeneity of the cations in the defect regions in $CuFe_{0.94}Ge_{0.06}S_2$.

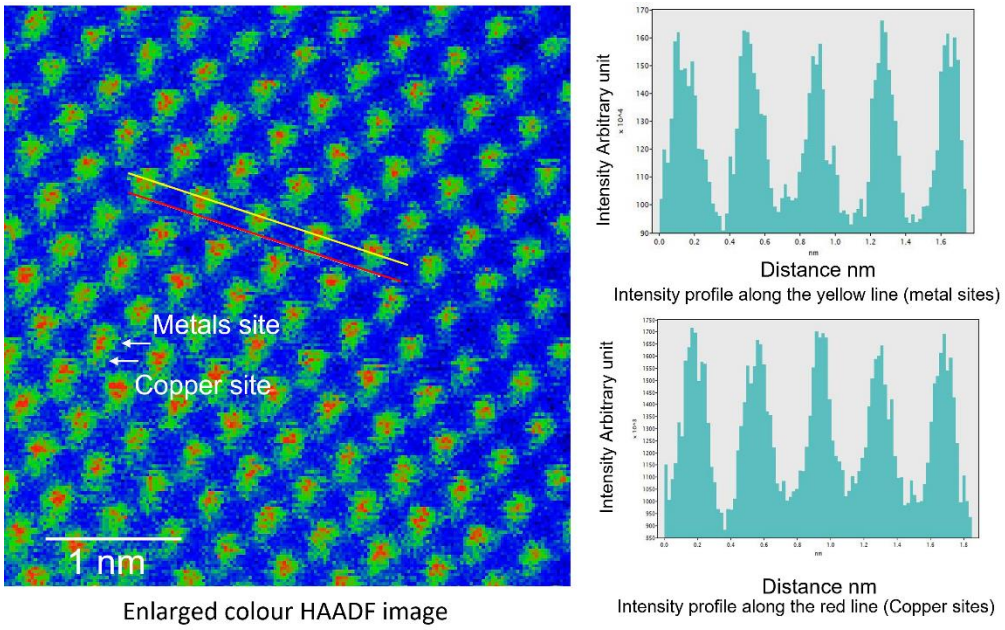


**Figure S5**. Enlarged HAADF-STEM image showing the uniform distribution of cations in $CuFe_{0.94}Ge_{0.06}S_2$.

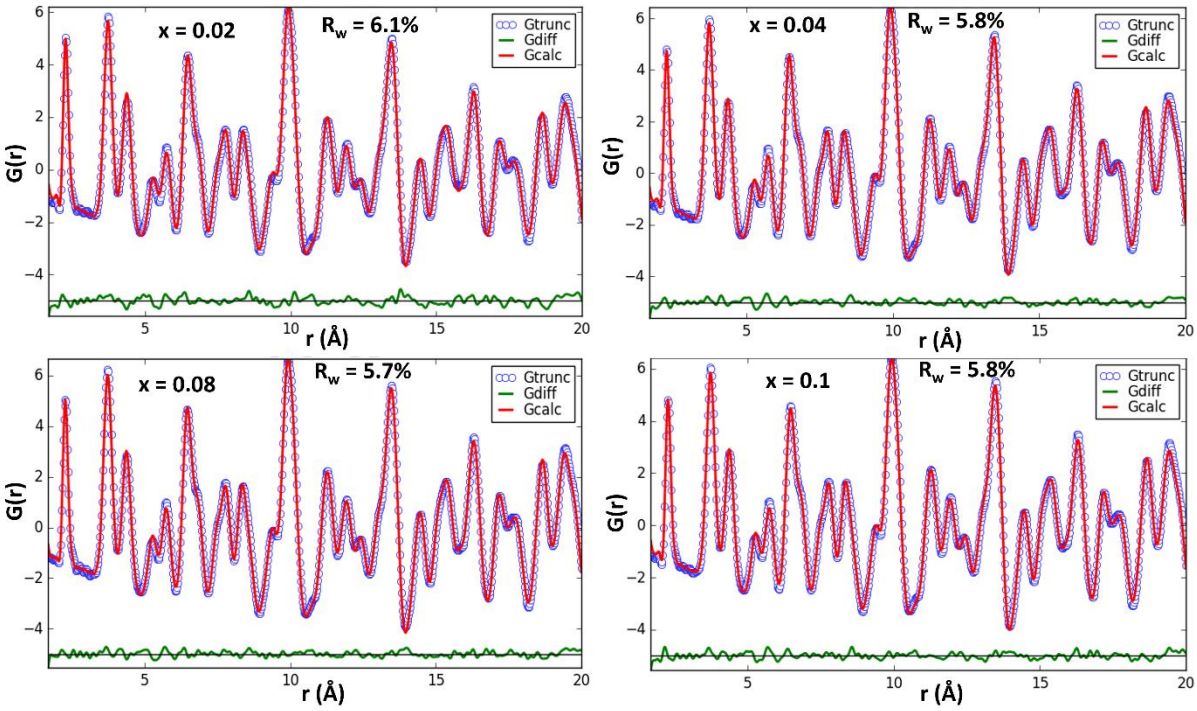


**Figure S6**. Experimental, calculated and difference pair distribution function, G(r) as a function of atomic-pair distance (r) for $CuFe_{1-x}Ge_xS_2$ ($0.02 \leq x \leq 0.1$).

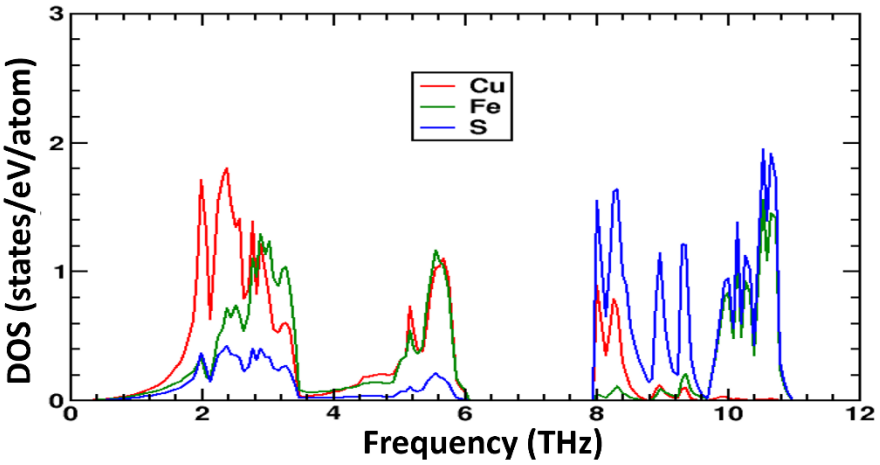


**Figure S7.** Phonon density of states (DOS) of $CuFeS_2$.

**Table S5**. Phonon group velocities of the LA, LA′ and TO modes in $CuFeS_2$and in $CuFeS_2$ with 6.25 at.% of Ge substitution.

| | **$CuFeS_2$ (m $s^{-1}$)** | **Ge-substituted $CuFeS_2$ (m $s^{-1}$)** |
|---|---|---|
| Γ – X | 2307, 2911, 5127 | 2470, 2553, 4723 |
| Γ – Z | 2009, 2921, 5271 | 2300, 2585, 5142 |
| Γ – N | 2352, 5354 | 2597, 4888 |

**Calculation Details:**

- **Lorenz number and electronic thermal conductivity**:

The electronic part of the thermal conductivity ($\kappa_e$) was calculated from the Wiedemann-Franz relation:

$$\kappa_e = L\sigma T \tag{S1}$$

$L$ is the temperature-dependent Lorenz number and $T$ is the temperature. The temperature-dependent Lorenz number was evaluated from the following relation:

$$L = \left(\frac{k_B}{e}\right)^2 \left( \frac{\left(r+\frac{7}{2}\right)F_{r+5/2}(\eta)}{\left(r+\frac{3}{2}\right)F_{r+1/2}(\eta)} - \left[\frac{\left(r+\frac{5}{2}\right)F_{r+3/2}(\eta)}{\left(r+\frac{3}{2}\right)F_{r+1/2}(\eta)}\right]^2 \right) \tag{S2}$$

Where $k_B$ is the Boltzmann's constant, $\eta$ is the reduced Fermi energy that is obtained from Seebeck coefficient values via the relation:

$$S = \pm \frac{k_B}{e}\left(\frac{\left(r+\frac{5}{2}\right)F_{r+3/2}(\eta)}{\left(r+\frac{3}{2}\right)F_{r+1/2}(\eta)} - \eta\right) \quad \text{(S3)}$$

Here, $F(\eta)$ is the reduced Fermi integral given by:

$$F_n(\eta) = \int_0^\infty \frac{x^n}{1+e^{x-\eta}}\, dx \quad \text{(S4)}$$

And $\eta = E_F/k_BT$ where $E_F$ denotes the Fermi level. Assuming that the main scattering mechanism is acoustic phonon scattering, the value of $r$ is taken as -1/2. The Lorenz number at each temperature value is therefore obtained by substituting $\eta$ and $r$ in equation (S2).

- **Mean sound velocity ($v_m$):**

$$v_m = \left[\frac{1}{3}\left(\frac{2}{v_t^3} + \frac{1}{v_l^3}\right)\right]^{-\frac{1}{3}}$$

and **average sound velocity ($v_{avg}$):**

$$v_{avg} = (2v_t + v_l)/3$$

where, $v_l$ and $v_t$ are the longitudinal and transverse sound velocities, respectively.

- **Shear modulus ($G$):**

$$G = dv_t^2$$

Where $d$ and $v_t$ are the density and transverse velocities respectively.

- **Young's modulus ($E$):**

$$E = \frac{dv_t^2\,(3v_l^2 - 4v_t^2)}{(v_l^2 - v_t^2)}$$

- **Debye temperature ($\theta_D$):**

$$\theta_D = \frac{h}{k_B}\left(\frac{3N}{4\pi V}\right)^{1/3} v_m$$

where $h$ is the Plank's constant, $k_B$ is the Boltzmann's constant, $N$ is the number of atoms in the unit cell, $V$ is the volume of the unit cell and $v_m$ is the mean sound velocity.

- **Distortion Parameters:**

Bond distortion parameter:

$$\gamma_x = \frac{1}{4}\sum_{i=1}^{4}\left[\frac{\langle x_i\rangle - x_i}{\langle x_i\rangle}\right]^2$$

where $\langle x_i\rangle$ and $x_i$ denote the mean and individual Ge-S bond lengths in the $GeS_4$ tetrahedra.

Angle distortion parameter:

$$\gamma_\theta = \frac{1}{6}\sum_{i=1}^{6}\left[\frac{\langle \theta_i\rangle - \theta_i}{\langle \theta_i\rangle}\right]^2$$

where $\langle \theta_i\rangle$ and $\theta_i$ denote the mean and individual S-Ge-S bond angles in the $GeS_4$ tetrahedra.

- **Scattering Parameters:**

The point defect parameter ($A$) can be written as:

$$A = \frac{\Omega_o}{4\pi v_m^3}\Gamma$$

where, $\Omega_o$ is volume of the primitive unit cell, and $\Gamma = \Gamma_M$ (mass-difference fluctuation) + $\Gamma_S$ (strain-field fluctuation) given by:

$$\Gamma_M = \frac{\sum_{i=1}^{n} c_i\left(\frac{\overline{M_i}}{\overline{M}}\right)^2 f_i^2 f_i^2\left(\frac{M_i^1 - M_i^2}{\overline{M_i}}\right)^2}{\sum_{i=1}^{n} c_i}$$

and,

$$\Gamma_S = \frac{\sum_{i=1}^{n} c_i\left(\frac{\overline{M_i}}{\overline{M}}\right)^2 f_i^2 f_i^2 \varepsilon\left(\frac{r_i^1 - r_i^2}{\overline{r_i}}\right)^2}{\sum_{i=1}^{n} c_i}$$

where, $\overline{M_i} = \sum_k f_i^k M_i^k$ ; $\overline{r_i} = \sum_k f_i^k r_i^k$ ; $\bar{\bar{M}} = \frac{\sum_{i=1}^{n} c_i \overline{M_i}}{\sum_{i=1}^{n} c_i}$. Here $n$ is the number of crystallographic sub-lattices which is 3 for $CuFeS_2$ and $c_i$ is the degeneracy of each site in the primitive unit cell ($c_1 = c_2 = 1$, $c_3 = 2$ corresponding to Cu, Fe and S sites respectively). $\overline{M_i}$ and $\overline{r_i}$ denote the average mass and radius of the atoms on the $i^{th}$ sublattice, respectively. $M_i^k$ and $f_i^k$ are the atomic mass and fractional occupation of the $k^{th}$ atom on the $i^{th}$ sublattice, respectively. $\bar{\bar{M}}$ is the total average atomic mass of the compound. $\varepsilon$ is a phenomenological adjustable parameter that was evaluated from fitting Equation 1 to the experimental $\kappa_L$. For $CuFe_{1-x}Ge_xS_2$ samples, on the basis of germanium substitution occurring at the iron site, the total scattering parameter can be, thus, written as:

$$\Gamma = \frac{1}{4}\left(\frac{\bar{M}_{Fe}}{\bar{\bar{M}}}\right)^2 x(1-x)\left[\left(\frac{M_{Fe}^{Fe} - M_{Fe}^{Ge}}{\bar{M}_{Fe}}\right)^2 + \varepsilon\left(\frac{r_{Fe}^{Fe} - r_{Fe}^{Ge}}{\bar{r}_{Fe}}\right)^2\right]$$

**References**:


1. H. Xie, X. Su, G. Zheng, T. Zhu, K. Yin, Y. Yan, C. Uher, M. G. Kanatzidis and X. Tang, *Adv. Energy Mater.*, 2017, **7**, 1601299.
2. H. Xie, X. Su, S. Hao, C. Zhang, Z. Zhang, W. Liu, Y. Yan, C. Wolverton, X. Tang and M. G. Kanatzidis, *J. Am. Chem. Soc.*, 2019, **141**, 18900–18909.
3. S. Tippireddy, F. Azough, F. T. Tompkins, A. Bhui, R. Freer, R. Grau-crespo, K. Biswas, P. Vaqueiro and A. V Powell, *Chem. Mater.*, 2022, **34**, 5860−5873.
4. I. Nakai, Y. Sugitani, K. Nagashima and Y. Niwa, *J. Inorg. Nucl. Chem.*, 1978, **40**, 789–791.
5. A. Ghahremaninezhad, D. G. Dixon and E. Asselin, *Electrochim. Acta*, 2013, **87**, 97–112.
6. NIST X-ray Photoelectron Spectroscopy Database, Version 4.1 (National Institute of Standards and Technology, Gaithersburg, 2012); http://srdata.nist.gov/xps/.